Modelling and Simulation of a Flywheel Energy Storage System for Microgrids Power Plant Applications

CCTC 2015 Paper Number 1570034251

T. A. Theubou Tameghe[1], R. Wamkeue[2] and I. Kamwa[3]

[1]Université du Québec à Chicoutimi (UQAC), Québec, Canada
[2]Université du Québec en Abitibi-Témiscamingue (UQAT), Québec, Canada
[3]Institut de recherche d'Hydro-Québec (IREQ), Québec, Canada

Abstract

Answering the greenhouse gases emission reduction and environmentally friendly energy production policies, Microgrids (MGs) represent a new thought pattern with respect to the electricity service. Since, heterogeneous power sources are leveraged to power a local load, fluctuating production from renewable sources (e.g. solar or wind), combined with variable profile of the consumption, can cause system instabilities. This paper focuses on the modelling and simulation of a flywheel energy storage system (FESS). Its contribution in smoothing the power production profile is analyzed, and simulations results are discussed.

Keywords: microgrid; renewable energy; flywheel energy storage system; vector control; voltage and frequency stability, modelling and simulation.

Résumé

En réponse aux politiques de réduction des gaz à effets de serre et du développement des énergies propres, les micros réseaux (MRs) constituent une solution appropriée de production d'énergie électrique. Dans un tel système, des sources distribuées alimentent une charge locale. L'énergie fluctuante issue des sources renouvelables, combinée au profil variable de la charge peut être une cause d'instabilité de l'énergie produite. Cet article se penche sur la modélisation et la simulation d'un système de stockage d'énergie à roue inertielle. Sa contribution dans le filtrage du profil de puissance est étudiée et les résultats de simulations sont commentés.

Mots clés : micro-réseau; énergie renouvelable; system de stockage à roue inertielle; commande vectorielle, stabilité de tension et de fréquence, modélisation et simulation

1. Introduction

In the last decades, environmental policies adopted by much of industrialized countries, have led to the decentralization of production facilities and the integration of renewable-energy sources, such as solar and wind, which are inherently fluctuating [1]-[3]. The increasing number of stakeholders and varieties of electrical charges type is an additional source of fragility in power grids [2]. Accordingly, smart and decentralized energy production requirements have led to new grid paradigms such as the so-called microgrids (MGs) which attracted great interest.

MGs integrate distributed energy resources, diesel generators, micro-turbines, fuel cells, photovoltaic, storage devices and end-use loads into a single micro power network which can co-generate with a larger network or isolate itself during heavy contingencies on the host network. Thus, the issue of balancing energy supply and demand can be solved at smaller scales by selecting a suitable energy storage system [1]. The main improvements obtained from the incorporation of energy storage devices are: a) efficient exploitation of otherwise wasted amounts of energy and maximum exploitation of the local production potential; b) increased reliability of energy supply; c) reduced emissions through the optimum energy management and d) higher utilization of overhead power lines.

Although the fact that MGs are small-scale application of the smart grid concept, they don't have the natural high inertia of a continental network [2]. The storage device must quickly respond to restore power equilibrium in the system. In a large majority of studies carried on the dynamic stability of MG, the flywheel energy storage system (FESS) has been chosen as the most applicable technology to improve the stability in MGs [4]-[7].

In this paper, the modelling and simulation of a FESS are addressed. In section II, the FESS device is positioned with respect to the microgrid power plant. Then, the internal structure of a FESS device is analysed and the modelling of each of its subsystems is carried out in section III. Finally in section IV, simulation results of the implemented FESS model using Matlab/Simulink and discussions thereon are presented.

2. Energy storage in microgrids and power frequency control

2.1 Synoptic of microgrid under study

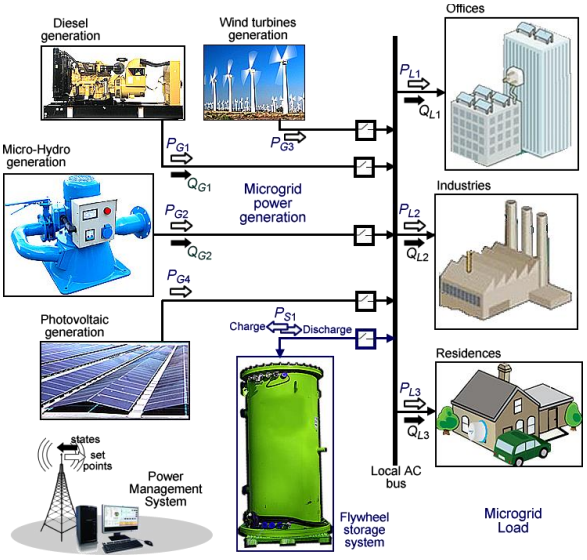

Figure 1. Microgrid system main components

The interconnection as well as the power flow between different components of a typical MG power plant is depicted in Fig.1. Diesel generation is usually used in remote areas due to its stability and fast installation. The other energy sources (Wind, Hydro and solar) are renewable

and some of them, in particular wind and solar, are characterized by their intermittence. To refine the power profile, FESS are used given their high efficiency, ability to switch rapidly between load (charge) and generator (discharge) states [3][4].

MG consumers are the local residential and industrial infrastructures with variable consumption profile. Operational parameters and variables of the MG devices (voltage, frequency, speed, torque, power, temperature, etc.) are monitored by the microgrid energy management system (MEMS). It evaluates in real time the power requirements in the MG and produces controls for an optimal system operation (in particular, a constant frequency and voltage operation).

2.2 Energy storage and active power balance requirement

In a MG generation plant, synchronous generators (SG) of diesel gensets and micro-hydro units are directly connected to the main AC bus. These SGs impose the system frequency and all connected SGs run at the same electrical speed ω_e. The system speed dynamics is therefore characterized by the swing equation given by (1) where $P_G = \sum P_{Gi}$, $P_L = \sum P_{Li}$ and $P_S = \sum P_{Si}$ are respectively the total instantaneous source, sink and FESS powers. J_T is the equivalent inertia of all connected SGs. In equation (1) as well as all the dynamic equations of this paper, $p(.)$ is the time derivative operator.

$$J_T\, p(\Delta\omega_e) = P_G - P_L - \Delta P_S \quad (1)$$

When the generation is balanced with the consumption (normal operation), the FESS power flow are disable, thus $\Delta P_S = 0$. Since $P_G = P_L$, it comes that $p(\Delta\omega_e) = 0$ and there is no variation of the system frequency. If there is a sudden decrease in power production, due to a drop in wind generation for example, the system frequency falls since each generator experiences a load step. Speed governor of each speed regulated generator increases fuelling (diesel) or water (hydro) flow to achieve a new generation/load balance. This native frequency regulation process can take from a few seconds to minutes during which, the system frequency may fluctuate in large proportions, given the low inertia of the MG machines [2]. By monitoring the MG AC bus frequency, the MEMS detects (or predicts) the frequency trends and operates the FESS to avoid extreme deviations. During this process, we have:

$$\Delta P_S \approx P_G - P_L \quad (2)$$

Similar analysis can be carried in the case of a sudden over-generation.

3. Modelling and control of the flywheel Energy Storage

3.1 Principle of operation

The FESS is a kinetic energy storage device in which energy is stored in the rotating mass of a flywheel. Fig. 2 shows the overall structure of a FESS connected to a MG power plant. The inertial mass is driven by an induction machines (IM) operating either in motor or generator. The

stored energy density E_{vol} is given by (3) where $\sigma_r = \rho(l\omega_m)^2$ is the radial tensile stress applied to the flywheel. ρ is the material density, ω_m the spinning angular speed and l the circular path radius of the considered elementary volume [7][8]. The coefficient K_F is related to the flywheel shape. By combining mass and volume density, the maximum storable energy is given by (4) where V is the flywheel volume and J its inertia.

$$E_{vol} = 0.5 K_F \sigma_r \tag{3}$$

$$E_{k\max} = 0.5 J \omega_{R\max}^2 \quad \Rightarrow \quad E_{k\max} = 0.5 K_F V \sigma_{r\max} \tag{4}$$

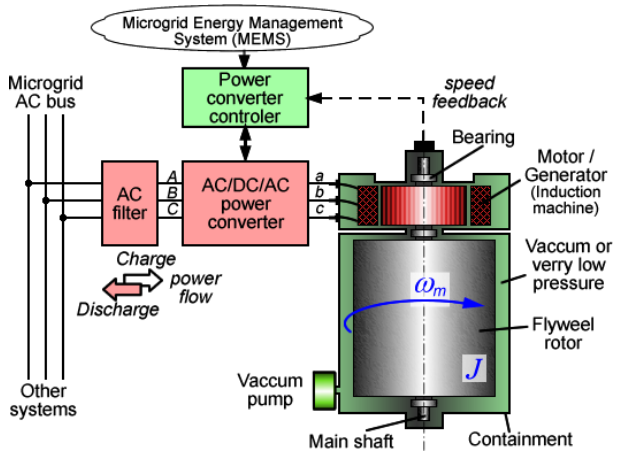

Figure 2. Flywheel energy storage system structure

Charge and discharge operations are related to the acceleration and deceleration of the flywheel, actuated by the IM. The state equation of the mechanical part of the FESS is given by (5). T_m is the induction machine torque and T_R the total friction (loss) torque, that can be minimized through the use of magnetic bearings (bearingless designs [8]).

$$J \frac{d\omega_m}{dt} = T_m - T_R \tag{5}$$

3.2 Induction machine dynamic model

The IM is generally a squirrel cage induction machine (SCIM) thanks to its low-cost and reliability [7]. For accurate control of torque (or power) of this machine, its dynamic equations are written in a synchronously rotating dq-reference frame. The SCIM's fluxes and voltages basic equations are given by (6) and (7) respectively. The corresponding equivalent circuits are shown in Fig.3. Quantities are expressed in SI units. R_a and R_A are respectively the resistances of the stator windings and the rotor bars. $L_s = L_a + L_m$, $L_r = L_A + L_m$ and L_m are the stator, rotor and magnetizing inductances respectively. ω_s is the dq-frame rotating speed.

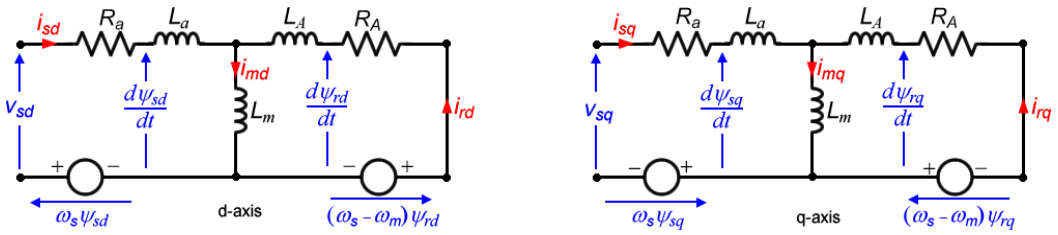

Figure 3. Induction machine equivalent circuit in the dq-frame

Since currents $I_r=[i_{rd} \quad i_{rq}]^T$ and the fast varying stator fluxes $\Psi_s=[\psi_{sd} \quad \psi_{sq}]^T$ are not of primary importance from the control viewpoint, they can be eliminated from the SCIM equations. By taking the fluxes matrix equation (6), expressions of stator fluxes and rotor currents in terms of other variables in the system are given by (8), where σ is the total leakage factor. Replacing (8) in dynamic equation (7) yields a more instructive state equation of the IM given by (9). $g\omega_s=\omega_s-\omega_m$ is the difference ("*slip*") between rotor and synchronous speed. IM's time constants are given by (10).

$$\begin{bmatrix}\psi_{sd}\\ \psi_{sq}\\ \psi_{rd}\\ \psi_{rq}\end{bmatrix}=\left[\begin{array}{cc:cc} L_s & 0 & L_m & 0\\ 0 & L_s & 0 & L_m\\ \hdashline L_m & 0 & L_r & 0\\ 0 & L_m & 0 & L_r\end{array}\right]\begin{bmatrix}i_{sd}\\ i_{sq}\\ i_{rd}\\ i_{rq}\end{bmatrix} \tag{6}$$

$$p\begin{bmatrix}\psi_{sd}\\ \psi_{sq}\\ \psi_{rd}\\ \psi_{rq}\end{bmatrix}=-\left[\begin{array}{cc:cc} R_a & 0 & 0 & 0\\ 0 & R_a & 0 & 0\\ \hdashline 0 & 0 & R_A & 0\\ 0 & 0 & 0 & R_A\end{array}\right]\begin{bmatrix}i_{sd}\\ i_{sq}\\ i_{rd}\\ i_{rq}\end{bmatrix}+\left[\begin{array}{cc:cc} 0 & -\omega_s & 0 & 0\\ \omega_s & 0 & 0 & 0\\ \hdashline 0 & 0 & 0 & -(\omega_s-\omega_m)\\ 0 & 0 & (\omega_s-\omega_m) & 0\end{array}\right]\begin{bmatrix}\psi_{sd}\\ \psi_{sq}\\ \psi_{rd}\\ \psi_{rq}\end{bmatrix}+\begin{bmatrix}v_{sd}\\ v_{sq}\\ 0\\ 0\end{bmatrix} \tag{7}$$

$$\begin{bmatrix}i_{rd}\\ i_{rq}\end{bmatrix}=\frac{1}{L_r}\begin{bmatrix}\psi_{rd}\\ \psi_{rq}\end{bmatrix}-\frac{L_m}{L_r}\begin{bmatrix}i_{sd}\\ i_{sq}\end{bmatrix}\Rightarrow\begin{bmatrix}\psi_{sd}\\ \psi_{sq}\end{bmatrix}=\sigma L_s\begin{bmatrix}i_{sd}\\ i_{sq}\end{bmatrix}+\frac{L_m}{L_r}\begin{bmatrix}\psi_{rd}\\ \psi_{rq}\end{bmatrix} \quad \text{with} \quad \sigma=1-\frac{L_m^2}{L_sL_r} \tag{8}$$

$$\Rightarrow p\begin{bmatrix}i_{sd}\\ i_{sq}\\ \psi_{rd}\\ \psi_{rq}\end{bmatrix}=\left[\begin{array}{cc:cc} \frac{-1}{T_a} & \omega_s & \frac{1-\sigma}{\sigma L_mT_r} & \frac{(1-\sigma)\omega_m}{\sigma L_m}\\ -\omega_s & \frac{-1}{T_a} & \frac{(\sigma-1)\omega_m}{\sigma L_m} & \frac{1-\sigma}{\sigma L_mT_r}\\ \hdashline \frac{L_m}{T_r} & 0 & \frac{-1}{T_r} & g\omega_s\\ 0 & \frac{L_m}{T_r} & -g\omega_s & \frac{-1}{T_r}\end{array}\right]\begin{bmatrix}i_{sd}\\ i_{sq}\\ \psi_{rd}\\ \psi_{rq}\end{bmatrix}+\frac{1}{\sigma L_s}\begin{bmatrix}1 & 0\\ 0 & 1\\ \hdashline 0 & 0\\ 0 & 0\end{bmatrix}\begin{bmatrix}v_{sd}\\ v_{sq}\end{bmatrix} \tag{9}$$

With $T_a=\dfrac{\sigma T_sT_r}{T_r+(1-\sigma)T_s}$; $T_s=\dfrac{L_s}{R_a}$ and $T_r=\dfrac{L_r}{R_A}$ (10)

The electromagnetic torque produced by the SCIM, which is a key quantity for any SCIM control strategy definition, is given by (11). It actuates the flywheel's speed through the earlier given equation (5).

$$T_{em} = \frac{3n_p}{2}\frac{L_m}{L_r}\left(\psi_{rd} i_{sq} - \psi_{rq} i_{sd}\right) \quad (11)$$

3.3 Power converters dynamic models

The power converter structure is shown in Fig. 4. It consists of two bidirectional voltage sourced inverters (VSI) connected by a dc-link having a high-value filtering capacitor C_{dc}. Each VSI has its own control scheme. The motor side VSI manages the power flow between the dc-link and the IM according to the power set points issued by the MEMS, and the grid side converter manages the power flow between the dc-link and the microgrid by regulating the voltage across the filtering capacitor C_{dc}.

When a positive power set point P_{ref} (i.e. charge command) is issued by the MEMS, the IM acceleration power is drawn from the dc-link and the capacitor's voltage drops. To suppress this voltage drop, the grid side VSI absorbs power from the MG and the acceleration power is finally drawn from the MG. For a negative P_{ref} (i.e. discharge command), the IM braking power raises the dc-link voltage and grid side VSI reacts by transferring this braking power to the grid. Thus, the motor side VSI is the master converter and the grid side VSI operates as a follower.

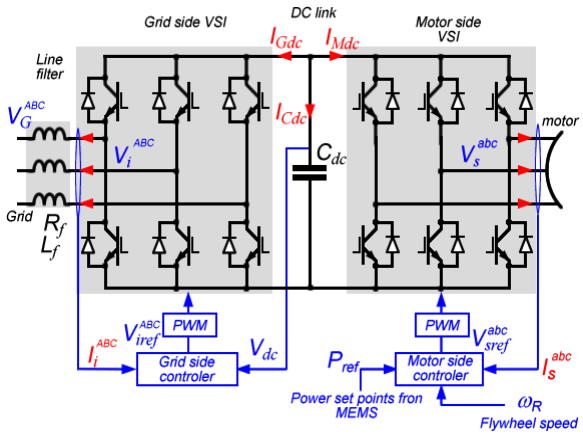

Figure 4. The back-to-back power converter

3.3.1 Motor side converter control scheme

Since the flywheel is mainly driven by the IM torque as stated by (5), the direct torque control, (DTC) and the Flux oriented vector control (FOC) schemes are the two commonly used control scheme for the motor side VSI. They are particularly addressed in [7]. Despite intuitiveness of the direct torque control (DTC) scheme it has, nevertheless, two main weaknesses [9]: a) steady-state errors induced by hysteresis controllers are hard to suppress and b) the variable

switching frequency of the VSI yield a complex spectral composition of the generated torque and so, causes serious concerns in torsional resonances avoidance.

The principal advantage of the FOC is a decoupled control of the IM rotor flux ψ_r and electromagnetic torque T_m to achieve high dynamic performance [7], [9]. The main idea is to transform the IM torque expression given by (11) to make the IM operating like a separately excited dc-machine, which is the quintessential electrical actuator. To achieve that, the dq-frame is chosen to get the rotor flux vector Ψ_r aligned with the d-axis so that the rotor's flux vector components are $\psi_{rd} = \psi_r$ and $\psi_{rq} = 0$. Rewriting the previous IM torque given by (13) leads to (12) which is similar to the dc-machine's torque. Hence, the IM torque is controlled by i_{sq}.

$$T_m = K_\psi i_{sq} \quad \text{with} \quad K_\psi = \frac{3n_p}{2}\frac{L_m}{L_r}\psi_r \tag{12}$$

This orientation of the rotor flux vector applied to the IM state equations given by (9) leads to the three transfer functions given by (13) and (14). It can be seen that the magnetizing flux ψ_r is related to the d-axis current i_{sd}, which is itself related to the d-axis stator voltage v_{sd} as given in (15). In the same way, the q-axis current i_{sq} is related to the q-axis command voltage v_{sq} also defined in (15) and is proportional to the desired torque. Thus, torque and flux control are obtained by two nested control loops as shown in Fig.5.

$$\psi_r = \frac{L_m}{1+sT_r} i_{sd} \tag{13}$$

$$i_{sd} = \frac{K_a}{1+sT_a} v_{cd} \quad \text{and} \quad i_{sq} = \frac{K_a}{1+sT_a} v_{cq} \quad \text{with} \quad K_a = \frac{T_a}{\sigma L_s} \tag{14}$$

$$v_{sd} = v_{cd} - \sigma L_s \omega_m i_{sq} \quad \text{and} \quad v_{sq} = v_{cq} + \sigma L_s \omega_m i_{sd} \tag{15}$$

Since the rotor's flux magnitude is regulated, its derivative is nil. The Park's angle θ_s, giving the flux vector position, is obtained from the q-axis rotor flux equation (9). Hence the dq-frame speed ω_s and the corresponding angle expressions are given by (16).

$$\omega_s = \frac{L_m}{T_r \psi_r^{ref}} i_{sq} + \omega_m \quad \text{and} \quad \theta_s = \int \omega_s dt \tag{16}$$

Since the storage is based on the kinetic energy, the IM's torque is indirectly controlled by the speed loop. The instantaneous stored energy in the flywheel is given by first equation in (17) yields the speed reference given by the second equation in (17).

$$E_K = \frac{J}{2}\omega_m^{*2} = \int P_{ref} dt \quad \Rightarrow \quad \omega_m^* = \sqrt{\frac{2}{J}\int P_{ref} dt} \tag{17}$$

The design of the proportional-integral (PI) controllers appearing in Fig. 5 is intensively addressed in [10] and [11]. The inner current controllers (PI2 and PI4) are designed by finding the balance between fast responses and good stability margins. The main risk of instability comes from the delays introduced by the PWM switching [11]. To avoid mutual influences between nested control loops, the outer loops (PI1 and PI3) are designed to be at least ten times slower than the inner ones. The dynamic responses of the latter can be therefore neglected in speed, flux and voltage PI-controllers design.

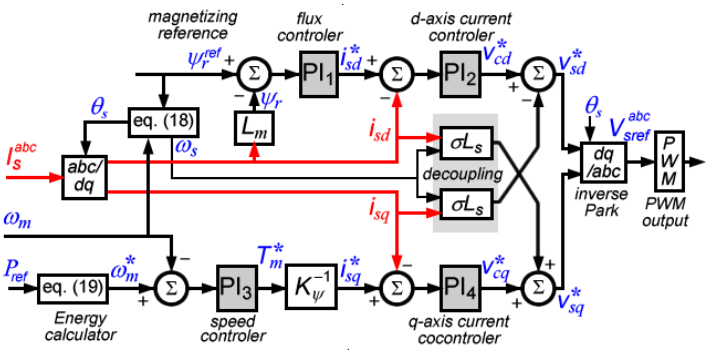

Figure 5. Motor side converter control scheme

3.3.2 Grid side control scheme

In the same way as for the motor side VSI control, this control is constructed using a grid side DQ-frame transformation. From the grid side VSI output point of view (see Fig.4) the whole microgrid is seen as a synchronous generator having L_f and R_f as stator leakage inductance and resistance. Then, the AC bus phase voltage is the derivative of a virtual grid flux Ψ_G as given by (18). The grid side DQ-frame is attached to the space phasor of the grid's flux and the currents $I_i = [i_{iD} \quad i_{iQ}]^T$ injected by the VSI is given by (19)-(20). This equation is quite similar to the state equation of currents obtained for the IM in (11). It comes that the two VSI control schemes are almost the same.

$$p(\Psi_G^{ABC}) = V_G^{ABC} \tag{18}$$

$$p\begin{bmatrix} i_{iD} \\ i_{iQ} \end{bmatrix} = \begin{bmatrix} \frac{-1}{T_f} & \omega_e \\ -\omega_e & \frac{-1}{T_f} \end{bmatrix} \begin{bmatrix} i_{iD} \\ i_{iQ} \end{bmatrix} + \frac{1}{L_f} \begin{bmatrix} 0 & \omega_e \\ -\omega_e & 0 \end{bmatrix} \begin{bmatrix} \psi_{GD} \\ \psi_{GQ} \end{bmatrix} + \frac{1}{L_f} \begin{bmatrix} 0 & \omega_e \\ -\omega_e & 0 \end{bmatrix} \begin{bmatrix} v_{iD} \\ v_{iQ} \end{bmatrix} \tag{19}$$

With $T_f = \frac{L_f}{R_f}$ (20)

If the virtual flux Ψ_G is orientated in the D-axis direction so that $\psi_{GD} = \psi_G$ and $\psi_{GQ} = 0$, the instantaneous powers injected by the grid side VSI are given by (21). It follows that, the active power P_G can be controlled by i_{iQ} and the reactive power Q_G by i_{iD}. The transfer functions of

the injected currents are given by (22). The VSI reference voltages supplied to the PWM modulator are given by (23). The DQ transformation angle is obtained using the virtual flux calculator which formula is given by (24). Despite the effectiveness of this formula, one can note that any dc offset—unavoidable in practice—inevitably leads to the integrator saturation (drift problem of the integrator [12]). A low-pass filter based estimator developed in [12] has been used for this work.

$$P_G = \frac{3\omega_e \psi_G}{2} i_{iQ} \quad \text{and} \quad Q_G = \frac{3\omega_e \psi_G}{2} i_{iD} \tag{21}$$

$$i_{iD} = \frac{1/R_f}{1+sT_f} v_{cD} \quad \text{and} \quad i_{iQ} = \frac{1/R_f}{1+sT_f} v_{cQ} \tag{22}$$

$$v_{iD} = v_{cD} - L_f \omega_e i_{iQ} \quad \text{and} \quad v_{iQ} = v_{cQ} + L_f \omega_e i_{iD} \tag{23}$$

$$\begin{bmatrix} \psi_{G\alpha} \\ \psi_{G\beta} \end{bmatrix} = \int \left(\begin{bmatrix} v_{i\alpha} \\ v_{i\beta} \end{bmatrix} - R_f \begin{bmatrix} i_{i\alpha} \\ i_{i\beta} \end{bmatrix} \right) dt - L_f \begin{bmatrix} i_{i\alpha} \\ i_{i\beta} \end{bmatrix} \tag{24}$$

$$\Rightarrow \psi_G = \sqrt{\psi_{G\alpha}^2 + \psi_{G\beta}^2} \quad \text{and} \quad \theta_G = \tan^{-1}\left(\psi_{G\beta} / \psi_{G\alpha}\right) \tag{25}$$

The Q-axis reference current is provided by the dc-link voltage's control loop. The transfer function relating the Q-axis current and the dc voltage is given by (26). The variable E_{dc} is a measure of the energy stored in the dc-link capacitor. One deduces the grid side VSI control scheme depicted in Fig. 6. PI controllers are designed using the same guidelines outlined earlier.

$$E_{dc} = \frac{-3\omega_e \psi_G}{sC_{dc}} i_{iQ} \quad \text{with} \quad E_{dc} = V_{dc}^2 \tag{26}$$

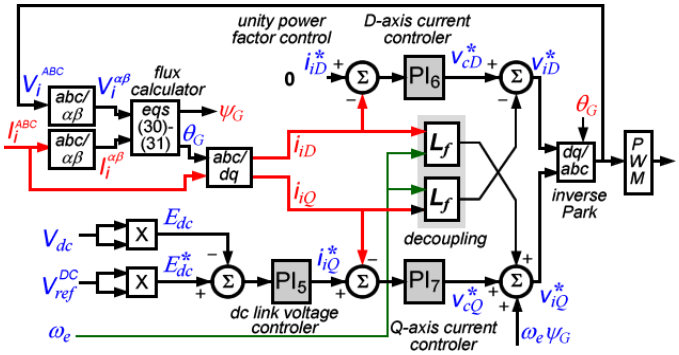

Figure 6. Motor side converter control scheme

4. Matlab/Simulink implementation and Simulation results

The previously analyzed FESS has been simulated using Matlab/Simulink (SimPowerSystem). The large inertia of the flywheel was implemented by increasing IM's rotor inertia. The main used parameters are given in Table 1. To emphasize the interaction between the different

subsystems, a succession of steps in power demand (MEMS power set points) was applied. The simulation starts with a power set point at zero. A charge command with a power of 10 kW is applied from $t = 10$ ms to $t = 0.5$ s, and a discharge command of 5 kW is applied from $t = 0.65$ s to $t = 0.42$ s. Between these events, a maintain command (i.e. $P_{ref} = 0$) is applied. It can be noted that all the process takes about 1 second, which allows us to simulate extreme stress on the storage device and its power smoothing capability. Fig. 7 shows compared plots of the IM, the grid-side VSI and the reference power profile. Curves show that the system responds accurately to the power charge/discharge requests. The grid power deviates somewhat from the reference given various losses across the conversion system.

The flywheel's speed obtained during the charge/discharge process is shown in Fig. 8. As discussed above, when the charge command is issued, the flywheel speed increases. This speed decreases for a discharge command, and remains constant for a zero power reference. The flywheel kinetic energy is calculated at each constant-speed. As expected, since the charge power is 10 kW and the discharge power is 5-kW, about half of the stored energy is retrieved, and the final speed is greater than the starting one.

Table 1. Simulation parameters

parameters		values	parameters		values
Microgrid			**Induction motor**		
3-phase voltage	V_{ll}	660/60 Hz	Rated values		460V/60Hz 37 kW
Power converter			Stator res.	R_s	0.0996 Ω
Filter ind.	L_f	10 mH	Rotor res.	R_r	0.0584 Ω
Filter res.	R_f	0.1 Ω	Stator ind.	L_a	0.87 mH
dc-link cap.	C_{dc}	4700 µF	Rotor ind.	L_A	0.87 mH
dc-link voltage	V_{dc}^{ref}	1200 V	Magnet. ind.	L_m	30.4 mH
PWM freq.	f_{PWM}	5 kHz	Rotor inertia	J	5 kg/m^2

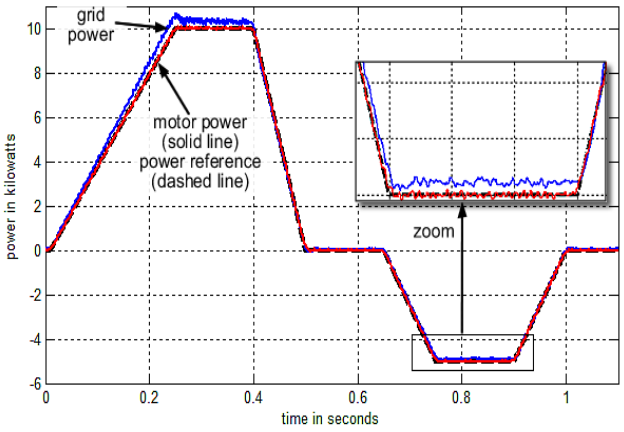

Figure 7. Power comparisons of the flywheel storage system

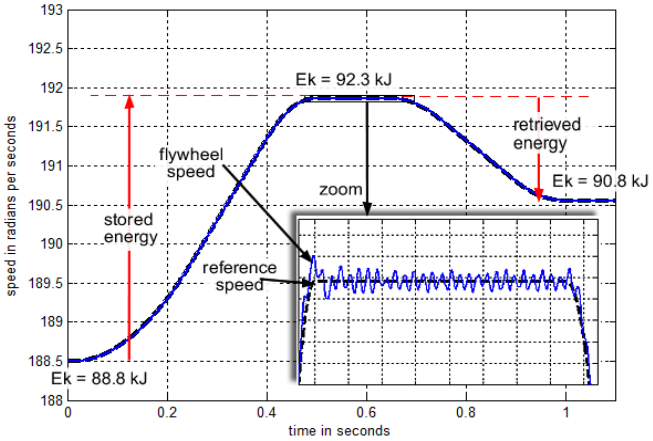

Figure 8. Comparisons between flywheel speed with the reference speed

5. CONCLUSION

In this paper, the analysis, modelling and simulation of a flywheel energy storage system have been presented. The Analysed FESS device was, firstly, divided into subsystems and each of them was modelled. The studied FESS was based on an induction motor actuator, on which was implemented a FOC control. The AC bus connection was done through a bidirectional inverter on with the virtual flux based control was used. All modelling stages were carried out. Developed models have been implemented using Matlab/Simulink software and obtained signals waveforms show good agreement with the developed theory.

6. References

[1] Molina, M.G., "Distributed energy storage systems for applications in future smart grids," *Transmission and Distribution: Latin America Conference and Exposition (T&D-LA), 2012 Sixth IEEE/PES* , pp.1-7, 3-5 Sept. 2012

[2] Xisheng T.; Wei D. and Zhiping Q., "Investigation of the Dynamic Stability of Microgrid," *IEEE Transactions on Power Systems* , vol.29, no.2, pp.698,706, March 2014

[3] Papadopoulos, T.A.; Papadopoulos, P.N.; Papagiannis, G.K.; Crolla, P.; Roscoe, A.J.; Burt, G.M., "Dynamic performance of a low voltage microgrid with droop controlled distributed generation," *Power and Energy Society General Meeting (PES), 2013 IEEE* , pp.1-5, 21-25 July 2013

[4] Diaz-Gonzalez, F.; Bianchi, F.D.; Sumper, A.; Gomis-Bellmunt, O., "Control of a Flywheel Energy Storage System for Power Smoothing in Wind Power Plants," *IEEE Transactions on Energy Conversion,* vol.29, no.1, pp.204-214, March 2014

[5] Samineni, S.; Johnson, B.K.; Hess, H.L.; Law, J.D., "Modeling and analysis of a flywheel energy storage system for voltage sag correction," *Electric Machines and Drives Conference, 2003. IEMDC'03. IEEE International* , vol.3, no., pp.1813-1818 vol.3, 1-4 June 2003

[6] Arghandeh, R.; Pipattanasomporn, M.; Rahman, S., "Flywheel Energy Storage Systems for Ride-through Applications in a Facility Microgrid," *IEEE Transactions* on *Smart Grid*, vol.3, no.4, pp.1955,1962, Dec. 2012

[7] Cimuca, G.; Breban, S.; Radulescu, M.M.; Saudemont, C.; Robyns, B., “Design and Control Strategies of an Induction-Machine-Based Flywheel Energy Storage System Associated to a Variable-Speed Wind Generator,” *IEEE Transactions on Energy Conversion*, vol.25, no.2, pp.526-534, June 2010

[8] Zhang, C.; wu, P.; Tseng, K.J., “FEM analyses for the design and modeling of a novel flywheel energy storage system assisted by integrated magnetic bearing, ” *IEEE International Conference on Electric Machines and Drives, 2005*, pp.1157-1164, 15-15 May 2005

[9] Casadei, D.; Profumo, F.; Serra, G.; Tani, A., “FOC and DTC: two viable schemes for induction motors torque control, ” *IEEE Transactions on Power Electronics*, vol.17, no.5, pp.779,787, Sep 2002

[10] Liuping Wang; Lu Gan, "A tutorial on PI velocity control of induction motors," *IECON 2012 - 38th Annual Conference on IEEE Industrial Electronics Society* , pp.1648,1653, 25-28 Oct. 2012

[11] Ho, W.K.; Hang, C-C; Zhou, J.H., "Performance and gain and phase margins of well-known PI tuning formulas," *IEEE Transactions on Control Systems Technology*, vol.3, no.2, pp.245-248, Jun 1995

[12] Idris, N.R.N.; Yatim, A.H.M., "An improved stator flux estimation in steady-state operation for direct torque control of induction machines," *IEEE Transactions on Industry Applications,* vol.38, no.1, pp.110-116, Jan/Feb 2002

7. Acknowledgements

This work was supported by the Industrial Innovation Scholarships (BMP Innovation) Program, offered jointly by CRSNG, FRQNT and IREQ.

8. Biography

Tommy A. Theubou Tameghe (S2010) received an MSc A. Degree from University of Quebec in Abitibi-Témiscamingue, Rouyn-Noranda, QC and is currently a Ph.D. student at the University of Quebec in Chicoutimi. The Thesis focuses on the analysis of integration techniques of distributed sources in actual power plants and smart grids.

René Wamkeue (S95, M98, and SM08) received the Ph.D. degree in electrical engineering from the École Polytechnique, Montreal, QC, Canada, in 1998. Since 1998, he has been with the Université du Québec en Abitibi-Témiscamingue (Qc), where he is currently a full professor of electrical engineering. His current research interests include control, power electronics, modelling, identification and diagnosis of electric machines, cogeneration and wind energy conversion systems. Prof. Wamkeue is a senior member of the IEEE/PES and acted as Secretary of the working group 7 for revision of IEEE Std-115.

Innocent Kamwa (IEEE Fellow, 2005) received the Ph.D. degree from Laval University, Québec City, QC, Canada, in 1988. He then joined Hydro-Québec's research institute (IREQ), where he is currently the chief scientist for Hydro-Québec's smart grid. He is a P. Eng. and Adjunct Professor of Power Systems Engineering at McGill University and Laval University. Dr. Kamwa serves on many IEEE/PES technical committees as member and officer, including the Fellow Evaluation, Electric Machinery, and Power System Stability committees.